Chapter 02 Literature survey

2.1 Preamble

The present chapter aims to review and highlight the contribution of the recent work on A-TIG welding process on various grades of stainless steel and alloy steel. This chapter involves mechanisms and forces associated with A-TIG welding process. Furthermore, effects of various weld parameters on weld bead geometry, microstructure and mechanical properties of A-TIG weld joint. Subsequently, multi-object optimization techniques applied to optimize the process parameters of the A-TIG welded joint in different grades of stainless steel are reported. Along with this, penetration enhancing variants of the A-TIG welding process such as Flux Bounded TIG (FB-TIG) and Flux Zone TIG (FZ-TIG) welding processes are summarized. Based upon this, a detailed literature review, key findings and the scope of the present research have been summarized.

2.2 Activated TIG welding mechanisms

There are various A-TIG welding mechanisms proposed by different researchers. Savitskii and Leskov in 1980 proposed the first mechanism, flux act as a surface-active agent that changes the surface tension of the molten weld pool, resulting in surface depression at the weld pool as shown in Figure 2.1. (Ahmadi & Ebrahimi, 2015). Moreover, it enhance the radius of curvature at the weld pool surface forms a minute cavity that supports the arc pressure and leads to penetration at low current in different grades of steel (Ahmadi & Ebrahimi, 2015; Vijay, et al., 2020) This mechanism is known as the TIG keyhole mode. However, very minute depression is reported in stainless steel at low weld current. The constriction of the arc due to electron attachment at the edge of the arc to form negative ions and enhances the current density at the anode arc root, which increases the weld penetration in weld metal than TIG weld noted in SS 316 LN and 304 (Patel, Badheka, Vora, & Upadhyay, 2019; Liu, et al., 2015), The constriction of arc has also been formed by the insulation effect of flux in stainless steel (Lowke, Tanaka, & Ushio, 2005). Heiple and Roper (1982) proposed a mechanism founded on the Marangoni effect in SS 21Cr-6Ni- 9Mn. The presence of surface-active elements (selenium, sulfur and oxygen) on the weld pool changes the temperature coefficient of surface tension from negative to positive (Yadaiah & Bag, 2013; Matsumoto, Misono, Fujii, & Nogi, 2005). Due to this change, the

fluid flows radially inward in the weld pool and has a relatively higher penetration depth (Mills K. C., Keene, Brooks, & Shirali, 1998; Rathod D.W., 2016; Leconte, Paillard, Chapelle, Henrion, & Saindrenan, 2006), This mechanism is known as the Reversal of Marangoni convection. Arc construction due to negative ions and arc constriction due to the insulation effect of flux and reversal Marangoni convection is the most acceptable phenomenon for higher penetration depth in A-TIG welding (Lowke, Tanaka, & Ushio, 2005; Leconte, Paillard, Chapelle, Henrion, & Saindrenan, 2006). Despite these studies, there are no defined standards for the A-TIG mechanism even though it is being used in a plethora of industrial applications.

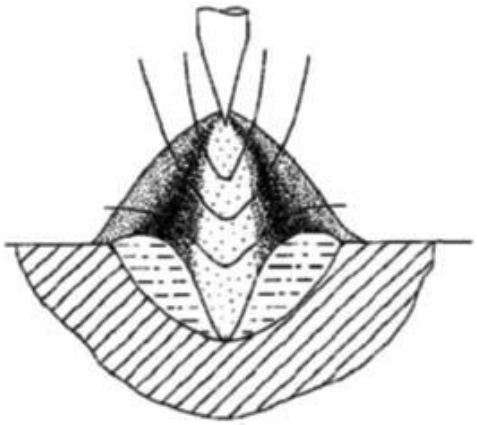

Figure 2.1 Keyhole mode (Ahmadi & Ebrahimi, 2015)

During the A-TIG welding process, the central ionized plasma-span gets reduced when the welding torch moves toward the flux covered surface from an uncovered surface. The vaporizing flux molecules like oxygen or halogens capture the electrons from the outer region of the plasma column due to their higher electron affinity. The concentration of a welding arc is augmented to a single point and the temperature increases which is known as constriction of the arc as shown in Figure 2.2 (Howse & Lucas, 2000). This rises the temperature at the anode thereby enhance the current density and the heat intensity. This increases the penetration depth in the A-TIG welding process (Kumar, Ahmad, & Singh, 2019).

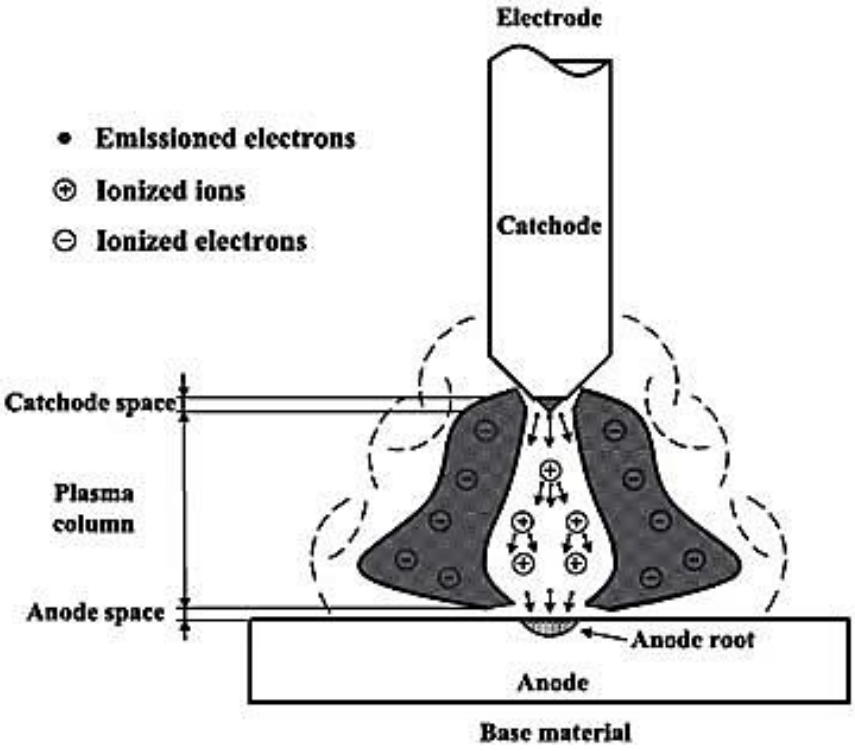

Figure 2.2 Schematic of arc constriction due to negative ions in the Activated TIG process (Howse & Lucas, 2000)

A layer of oxide flux acts as an insulating barrier to the arc current. At weld pool centre, the heat is sufficient enough to dissolve the flux. Hence, by the insulating effect of activated flux, the diameter of arc at the weld pool surface decreases. The density of heat at the centre of the weld pool increases at a specific current due to the insulating effect of the activated flux. The high heat input leads to an increase in pressure and magnetic pinch forces in the weld pool; thus, strong convective downwards flow in the weld pool can be observed in stainless steel (Lowke, Tanaka, & Ushio, 2005) Some of the elements that can be used as activated flux are Manganese Oxide (MnO_2), Titanium Dioxide (TiO_2), Molybdenum Dioxide (MoO_3), Silicon Dioxide (SiO_2) and Aluminum Oxide (Al_2O_3). The size of the particles can lie between 30 µm and 60 µm.

The arc constriction mechanism and its consequence on penetration with different halides in A-TIG welding was described by Skvortsov (1998). It was reported that partial pressure of electron gas changes with the addition of various halides, this result in a unique arc constriction. Tseng and Hsu (2011) investigated the heat energy requirement for TIG penetration and found that the heat required is reduced by spraying a thin coat of activated flux on the weld surface. Various activated fluxes with different particle sizes were mixed with acetone and then applied to a SS 316 L 6 mm thick plate. It was observed that during

A-TIG welding, the arc voltage rises, which conveys more heat input in welding process. Tanaka et al. (2000) found the wide regions of blue luminous plasma in A-TIG and TIG welding. In the case of TIG welding, the intense region was expanded in the lower part of the arc whereas, in the case of A-TIG welding, the intense region was only observed at the centre in the lower part of the arc. Tseng and Chen (2012) compared two activated fluxes: TiO_2 and SiO_2 on a SS 316 L. It was reported that the arc voltage was higher with SiO_2 than TiO_2 flux. This is attributed to the fact that SiO_2 has a higher electronegativity tendency as compared to TiO_2, which attracts more electrons from the outer boundary of the arc construction. A similar comparison was done by Venkatesan et al. (2017) on SS 304 L by using SiO_2, TiO_2 and tri- component fluxes comprising SiO_2, TiO_2 and Cr_2O_3. It was observed that the arc constriction was the dominant mechanism that caused the enhancement in the penetration. Also, the superiority of SiO2 was observed. The striations in the A-TIG welding plasma column increase the current density at the anode spot, which results in greater penetration of the welds (Huang H. , Shyu, Tseng, & Chou, 2006). From the review, it can be identified that vaporized activated flux has more electronegativity making the arc column more constricted. Marangoni convection was first identified by physicist James Thomson in 1855. A complete theoretical behavior was given by Gibbs in 1878. During the TIG welding process, the surface tension gradient decreases with an increase in temperature which promotes the Marangoni convection. Therefore, the fluid flow in the weld pool was observed in an outward direction. This leads to increase in width and reduced depth of the pool as depicted in Figure 2.3(a). Heiple et al. (1982) deliberated the effect of the activated flux on the fluid flow motion in the weld pool. The fluid flow direction in the weld pool is decided by the magnitude and direction of thermo-capillary forces controlled by the surface- active agent. It was reported that the surface-active agent of more than 500 ppm change the temperature coefficient of surface tension from negative to a positive value. Thereby reversing the Marangoni convection direction from edge to canter of the weld pool as shown in Figure 2.3(b). This phenomenon was observed in austenitic stainless steel, A-TIG welding process as activated flux act as a surface-active agent which is responsible for higher depth of penetration.

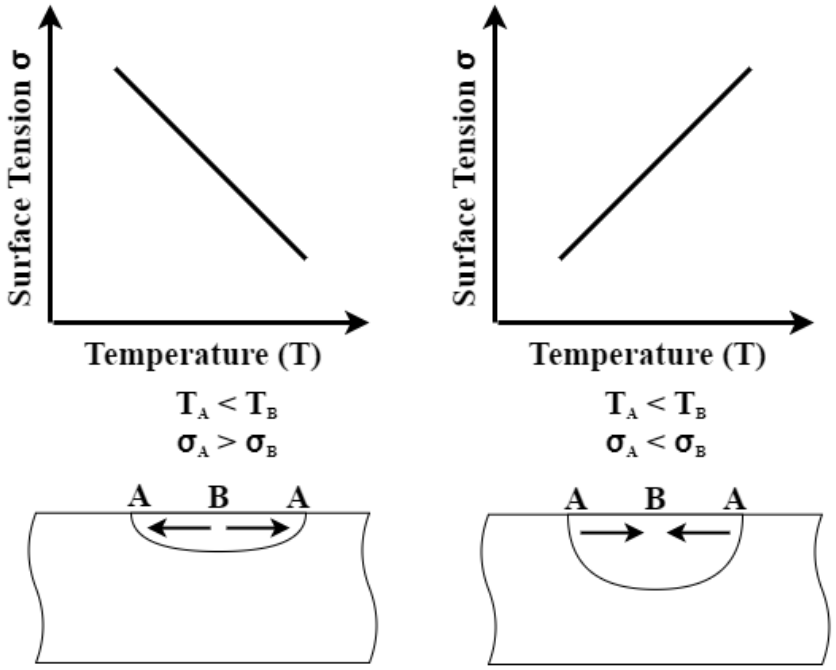

Figure 2.3 (a) Marangoni convection (B) Reversal Marangoni convection

2.3 Forces acting in activated TIG welding

The forces acting on the molten metal in a weld pool are Marangoni force, Lorentz force, buoyancy force, and aerodynamic drag force (Kou & Wang, 1986; Gibbs, 1878).

2.2.1 Marangoni forces

Marangoni forces take place due to the differences in the free surface energy of a fluid or a solid (Wang, Nates, Pasang, & Ramezani, 2015; Katopodes, 2019). This phenomenon is also known as thermo-capillary or surface-tension driven convection addressed by Wang et al. (Wang, Nates, Pasang, & Ramezani, 2015). The flow of the fluid is a function of surface tension gradient on the weld pool surface (Ahmadi, Ebrahimi, & Khosroshahi, 2013), The thermo-capillary flow can be identified using the Marangoni number (Ma) as given in equation (2.1) (Vidyarthy & Dwivedi, 2016).

$$Ma = \frac{d\gamma}{dt}\frac{dT}{dx}\frac{l^2}{\eta a} \tag{2.1}$$

Where,

dT/dx is temperature gradient,

dγ/dT is surface tension gradient,

a is the thermal diffusivity,

η is the dynamic viscosity,

l is the characteristic length.

In TIG welding process, the Marangoni force changes the pattern of fluid flow in an outward direction as shown in Figure 2.4(a). Therefore, the maximum heat is transferred to the wall of the weld pool which is responsible for shallow penetration. The reverse fluid flow pattern is reported in A-TIG welding as shown in Figure 2.4(b), which changes the weld pool geometry. Therefore, the Marangoni force is considered to be one of the most dominant forces for shaping the weld pool (Wang, Nates, Pasang, & Ramezani, 2015; Kumar, Ahmad, & Singh, 2019).

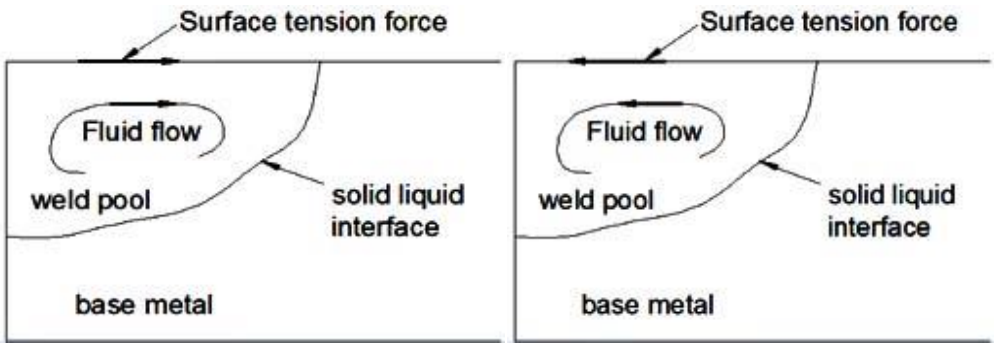

(a) **(b)**

Figure 2.4 Marangoni force in (a)TIG welding (b) Reverse Marangoni force in A-TIG welding

2.2.2 Lorentz force

Lorentz force takes place due to electric and magnetic force at a point due to electromagnetic fields. This acts on the welded region at the tip of the arc (Huang, Liu, Zhu, Hua, & Dong, 2020) In arc movement of TIG welding, the current asymmetry results in an electromagnetic force acting in the forward direction of the welding pool (Nemchinsky, 1996). At high arc speeds the value of electromagnetic force, which acts toward the canter of the weld pool and presses it down as shown in Figure 2.5(a). The Lorentz force ($\overrightarrow{Fem}$) is governed by the equation (2.2).

$$\overrightarrow{Fem} = \vec{J} \times \vec{B} \tag{2.2}$$

Where, $\vec{J}$ and $\vec{B}$ are the current density and magnetic flux in the weld pool respectively.

The weld pool shape majorly depends on Lorentz force when the surface tension gradient was negative (Berthier, Paillard, Carin, Valensi, & Pellerin, 2012).

2.2.3 Buoyancy force

The density of the liquid metal in the molten pool decreases with an increase in the temperature (Wang, Huang, Huang, Fan, & Guo, 2017) Due to differences in density, buoyancy force gets induced in the weld pool and the fluid tends to flow from low density to high density as shown in Figure 2.5(b). However, the effect of buoyancy forces is less compared to other forces acting during A- TIG welding. The buoyancy force calculated by Boussinesq approximation (B) is shown in equation (2.3).

$$B = -\rho g \beta \, (T - T0) \tag{2.3}$$

Where ϱ is the liquid metal density, g the gravitational acceleration constant, β coefficient of thermal expansion, T temperature of liquid metal and To reference temperature which is generally a room temperature.

2.2.4 Aerodynamic drag force

The aerodynamic drag force is induced as an outward surface flow due to the shearing force forms by the plasma stream which is also known as arc plasma force as shown in Figure 2.5(c) (Bordogna, et al., 2020) . The arc plasma force considerably increases at the long arc length as the momentum and kinetic energy level is lifted drastically due to the high welding current (Li, Chen, Zhang, Yang, & Lei, 2020). Mills and Knee (1990) developed the mathematical models to describe the effects of the above-mentioned forces on fluid flow and the temperature contours in the weld pool.

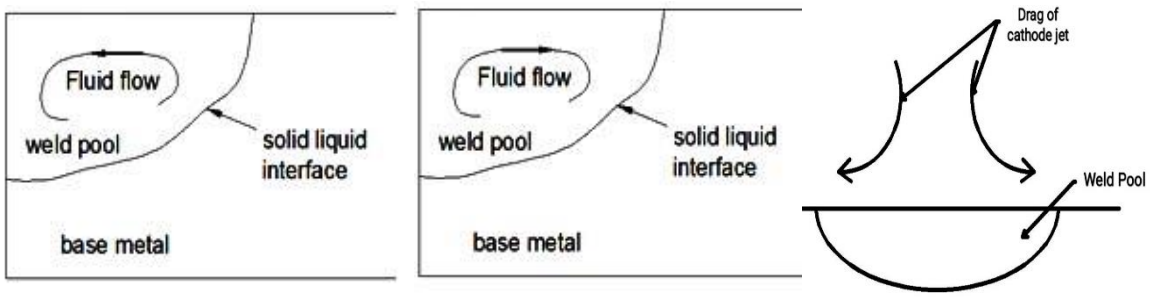

(a) **(b)** **(c)**

Figure 2.5(a) Electromagnetic force (b) Buoyancy force (c) Aerodynamic drag force

2.4 Consequence of process parameters on weld bead geometry of stainless steel TIG and activated TIG weld

The variables of the A-TIG welding process affect weld bead profile of weld metal and thereby quality of weld. The significant weld parameters are welding current, weld speed, arc voltage, arc length, electrode geometry, shielding gas composition and activated flux (Li, Zou, Yao, & Peng, 2017).

2.4.1 Welding current

The heat induced during the arc welding process is directly proportional to the welding current. Hence, both of these are key factors that influence weld penetration (Tathgir, Bhattacharya, & Bera, 2015). The heat flux density (Q) is calculated by the expression in equation (2.4).

$$Q = \frac{\eta VI}{2\sigma^2 \pi} \tag{2.4}$$

Where,

V is the welding voltage,

I is the welding current,

η is the arc efficiency,

σ is the width parameter at the anode root.

The close circuit current is directly proportional to heat flux density. Therefore, increase in weld current would increase the total heat input and the temperature gradient which results in high thermo-capillary convection (Song, Wang, Hu, Zhang, & Liang, 2018). However, larger currents are also responsible for higher electromagnetic and aerodynamic drag forces. Electromagnetic force makes the weld pool deeper, but aerodynamic drag force adversely affects the weld penetration and forms a wider weld pool. At high welding current, electromagnetic forces produced the significant stirring in weld pool and thereby create the vortex in weld pool which increase the weld penetration and reduce the bead width (Mills & Keene, 1990). Moreover, in A-TIG welding, due to the presence of surface-

active elements (sulfur and oxygen), reversal Marangoni convection as well as constriction of the arc phenomena were observed which dominate the effect of aerodynamic drag force (Vidyarthy & Dwivedi, 2016) Due to this, the fluid flows radially inward in weld pool. Hence, high penetration with lesser bead width were reported in A-TIG compared to TIG welding of SS 304 LN as shown in Figure 2.6. Moreover, improved penetration was reported in high sulfur steel than low sulfur steel with increasing the current. A similar result was noticed by Maduraimuthu et al. (2012) on P91 steel. A higher weld current changes the molten metal flow and subsequently the geometry of the weld pool by altering the strength of different forces acting during the welding process. It can be summarized that high weld current increases the penetration in the A-TIG welding process, but in the TIG welding, the penetration increases only up to a limit. Further increasing the current will lead to a wider weld width, but not the penetration depth.

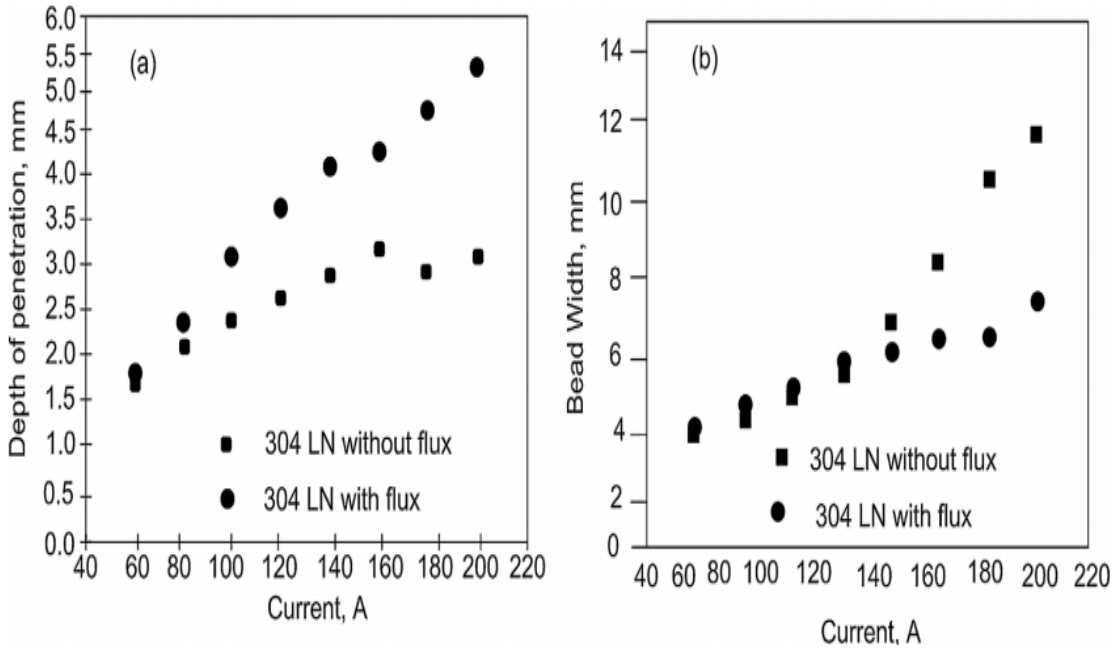

Figure 2.6 Disparity in weld metal geometry (a) penetration depth, (b) weld bead width with current, in 304LN stainless steel welds (Vidyarthy & Dwivedi, 2016)

2.4.2 Weld travel speed

The weld travel speed is the rate at which the arc moves along the base plate during the welding process. Torch speed is inversely proportional to total heat input per unit length of the weld that affects the geometry of the weld pool. Heat input (Hi) during the welding at any point is given by equation (2.5).

$$H_i = \frac{\eta VI}{S} \tag{2.5}$$

Where

ηVI is the total heat transfer to the weld surface

S is weld travel speed.

An increase in the torch speed reduces the net heat input per unit length, which reduces the weld pool cross-section area and subsequently welds pool geometry. The shape of a weld pool geometry is presented in terms of weld D/W ratio. At lower torch speed, temperature gradient increase which leads to an increase in D/W ratio in the high Sulfur steel (S > 70 ppm) and a decrease in the low Sulfur (S < 50 ppm) steel (Marya & Edwards, 2002). Tseng and Chuang (2012) reported that the penetration in 316 L SS is a function of welding current and torch speed. At a particular weld current, the penetration depth is inversely proportional to torch speed as shown in Figure 2.7. Lu et al. (2013) pointed out that if torch speed reduces, then penetration becomes deep and narrow. At lower torch speed, the arc has adequate time to blend oxygen in the weld pool that forms an oxide on the weld surface. This oxide decreases the surface tension of the weld pool resulting in shallow and wide weld pool profile. When the torch speed is increased, the total heat input at the weld zone decreases gradually; hence, Marangoni convection and weak electromagnetic force are produced which are responsible for the reduction in weld penetration (Bhattacharya, 2016).

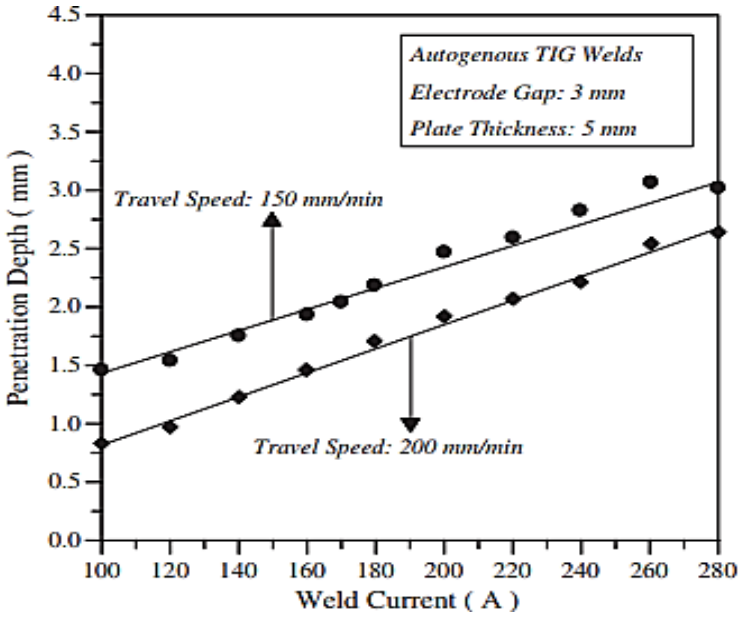

Figure 2.7 Torch speed effect on weld penetration with changing weld current (Tseng & Chuang, 2012)

2.4.3 Arc voltage

In TIG or A-TIG welding, an increase in arc voltage increases the heat input, leading to a higher D/W ratio for high sulfur and lower for low sulfur steel (Bhattacharya, 2016) and the arc voltage is affected by the geometry of the electrode (Bort & Franck, 2016). Chern et al. (2011) explained the effect on arc voltage with and without flux TIG welding on 2205 SS. Different oxide fluxes were compared and observed that the arc voltage was higher in A-TIG when compared to TIG welding as shown in Figure 2.8. This attributes to flux with nonmetal oxide (SiO_2) having higher resistivity compared to metallic flux (Al_2O_3) and without flux condition. Due to higher resistance, the conductive channel between the electrode tip and weld metal surface gets formed. The activated flux film gets evaporated by the arc heat and thereby creates the longer arc length result in high arc voltage. Li et al. (2007) reported the effect of SiO_2 and TiO_2 flux on the arc voltage of SS 1Cr18Ni9Ti. Figure 2.9 shows the waveform of arc voltage without flux and with flux (SiO_2 and TiO_2) at 150 A current. With SiO_2 flux, higher arc voltage was observed in A-TIG welding than TIG welding but in contrast with TiO_2 flux, arc voltage was slightly lower. The study concluded that changes in voltage depend on resistivity and conductivity of applied fluxes. A similar study was reported by Aniekan et al. (2017).

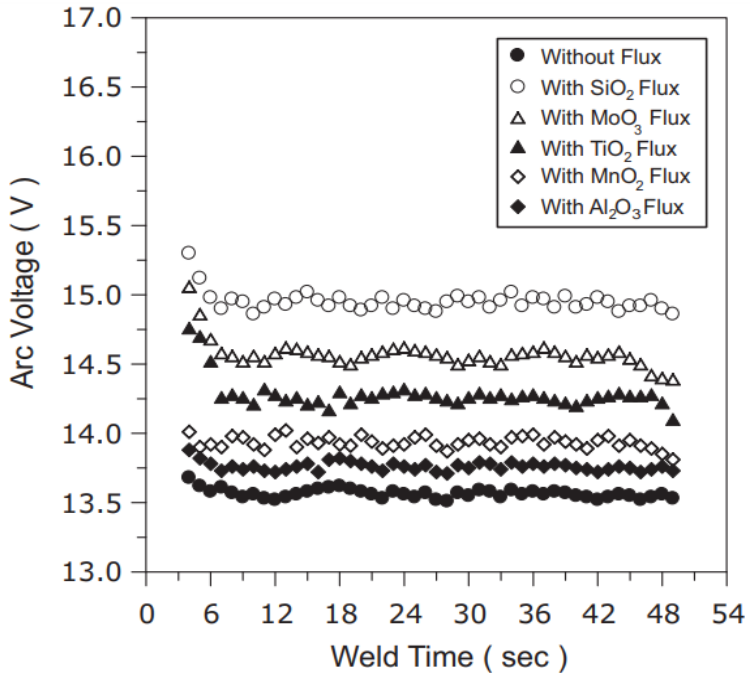

Figure 2.8 Effect of various oxide flux on arc voltage (Tseng & Hsu, 2011)

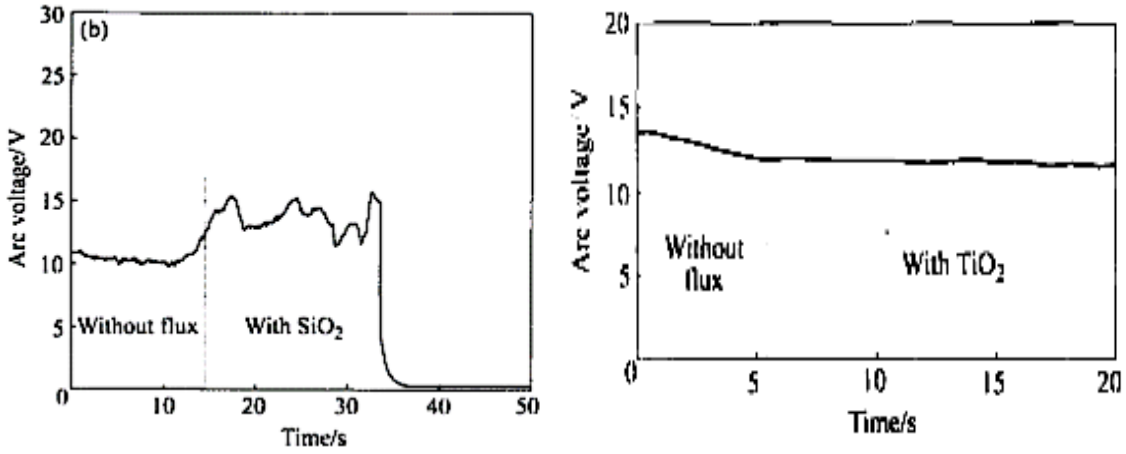

Figure 2.9 Arc voltage waveforms with (a) SiO_2 and (b) TiO_2 flux (Li, Wang, Zou, & Wu, 2007)

2.4.4 Arc length

During welding, an arc is formed between the electrode and weld metal due to the ionization of the gas. Arc length generally varies from 1 mm to 10 mm (Jaypuria, Mahapatra, Sahoo, & Jaypuria, 2020). Increasing the arc length and resistance to the flow of charged particles leads to higher voltage at a constant value of current (Rathod, Pandey, Aravindan, & Singh, 2017). When the arc length increases, the heat distribution area at the anode root becomes wider. Because of the wider arc of plasma in TIG welding, aerodynamic drag force increases, which makes the weld pool wider Increasing the arc length also reduces the overall arc efficiency because of an increase in the anode root area. Heat loss from the weld pool surface increases due to the more convection and radiation from the weld pool surface. Mills and Keene (1990) observed that increasing the arc length reduces the D/W ratio as shown in Figure 2.10. At higher arc length, thinner shielding gas protection to the weld pool becomes weak. It allows carbon dioxide to enter the outer layer of shielding gas and enhance the arc oxidizability. In this situation, surface- tension-induced convection becomes weaker due to oxide formed on the weld surface, and thus D/W ratio is adversely affected. Initially, with increasing arc length, the weld voltage increases which dominates the effect of anode root area, oxidizability of arc and heat loss from the plasma arc. But after reaching the optimal arc length, the above three parameters dominate the effect of weld voltage and form a wider and shallow weld pool.

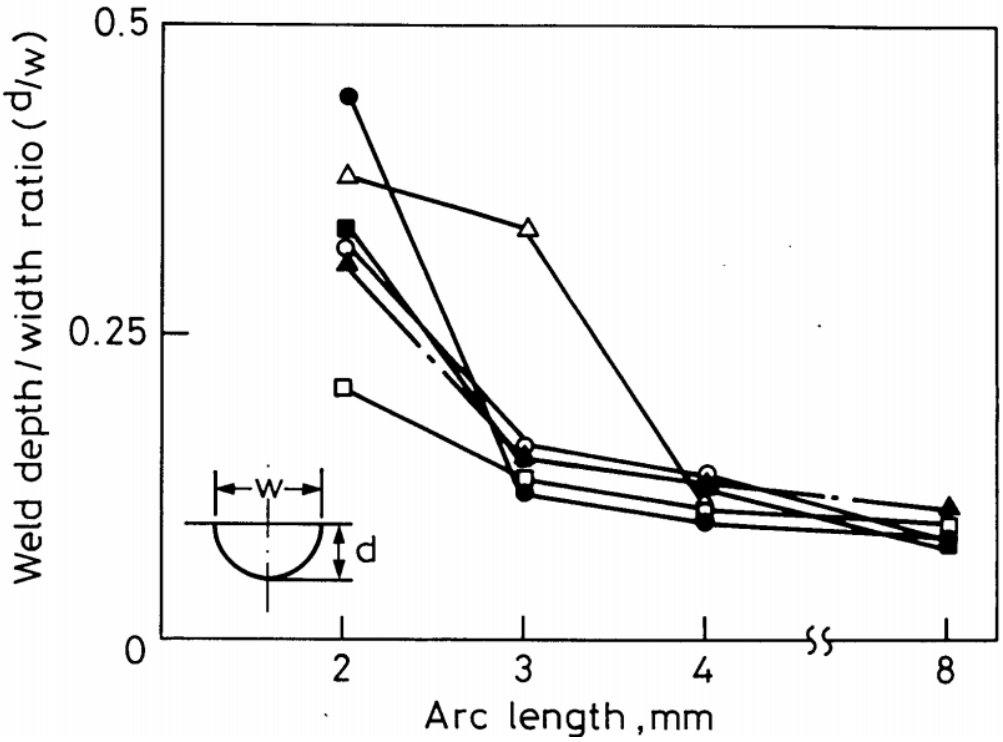

Figure 2.10 Effect on weld D/W ratio with an arc length of different steel casts; each mark signify a different steel (Chakravarthy, Agilan, & Neethu, 2019)

2.4.5 Welding electrode geometry

The welding electrode geometry plays a major role in the quality of the weld (Muzamil, et al., 2019) The geometry of the electrode such as electrode diameter, electrode tip angle and profile of the electrode (conical tipped, frustum and wedge shape electrode) may tend to change the arc pressure which affects the aerodynamic drag force and arc root area. In frustum and wedge shape electrodes, more uniform current distribution across the weld pool was observed compared to conical tipped electrodes thus resulting in lesser thermo-capillary and electromagnetic forces. The amount of arc pressure is inversely proportional to the cross-section of the flat surface of electrode (Mills & Keene, 1990; Poloskov, Erofeev, & Logvin, 2006).

When there is a conical tip electrode, increasing the electrode tip angle has a slight improvement in the heat distribution area at around 14% (Tsai & Eagar, 1985). The cross-section of the welded area and electron temperature reach a maximum value at an electron tip angle of 45°, but by either increasing or decreasing the tip angle, the electron temperature reduces with a slight variation in the current density (Tanaka, et al., 2006). The

alignment of the wedge shape electrode to weld direction has a major influence on the penetration due to the large variation in the temperature gradient and velocity produced by thermo-capillary forces. A 75° inclination of the weld electrode improves the penetration which attributes to an increase in strength of Lorentz force (Hiraoka, Okada, & Inagaki, 1985). Tseng et al. (2011) reported that activated flux increases the arc voltage and thus a reduction in the electrode diameter is observed with A-TIG than TIG welding. Therefore, to avoid electrode consumption in A-TIG welding, a larger diameter (3.2 mm) of an electrode is more suitable (Patel & Jani, 2020).

2.4.6 Shielding gas

Shielding gas used in TIG welding is inert or a semi inert gas. It shelters the weld pool from the atmosphere, controls the electrode temperature and stabilizes the electric arc. The selection of shielding gas influences the characteristics of the weld penetration profile. In accordance with the ionization potential of the shielding gas, heat flux and consequently the fusion zone area changes in the A-TIG welding process (Garasic, Kozuh, & Jurica, 2019). Generally, argon gas is used as a shield in TIG and A-TIG welding processes. Shielding gas directly influences the arc voltage; hence, the change in gas composition, the arc voltage also get changed (Huang H. , 2010).

The influence of oxygen addition in argon gas on SS 304 was examined by Lu et al. (2003) It was reported that the weld D/W ratio increases with addition of oxygen to the argon in the range of 3000 ppm to 5000 ppm at 10 l/min and 20 l/min flow rate. Oxygen contents below 2000 ppm or over 6000 ppm, the weld D/W ratio reduces to 0.2. The addition of oxygen forms oxide slag on the welded surface and also oxidizes the electrode tip inevitably. Burgardt and Heiple (1986) added helium in argon to TIG weld SS with sulfur doped and selenium doped conditions. It is reported that the D/W ratio reduces in SS 304 at a high amount of helium, whereas the D/W ratio increases in sulfur and selenium doped SS 304 with the addition of helium. This is attributed to the high conductivity of helium. However, helium is lighter than argon; hence, it requires high gas flow rate for proper shielding. Huang (2010) mixed hydrogen in pure argon which increased the arc voltage and thereby heat input to the work piece, which tends to increase the weld D/W ratio in A-TIG weld SS 304. Tathgir et al. (2015) reported that in A-TIG welding, the addition of 5% H_2 in argon increases the penetration by 70% in austenitic stainless steel with TiO_2 flux. However, Rodrigues and Loureiro (2005) also study the influence of argon, argon–helium

and argon–hydrogen mixture on the A-TIG weld of SS 316. In A-TIG weld with argon – hydrogen mixture, a considerable level of porosity was reported and it increases with an applied flux proportion but it was not observed with argon and argon–helium mixture. Huang (2009) examined the effect of nitrogen (2.5–10 vol.%) in argon as a shielding gas and reported that with the same weld parameters; the D/W ratio increased in TIG as well as in the A-TIG welding process. Burgardt and Heiple (1985) reported that the addition of a small quantity of concentrated SiO_2 to the pure argon shielding gas (700 ppm SiO_2 in the torch gas) significantly improves the TIG weld penetration on SS 304.

2.4.7 Activating flux

The spectacular increment in weld penetration is executed by spraying a thin layer of activated flux on the surface to be weld (Babbar, Kumar, Jain, & Gupta, 2019; Vidyarthy & Sivateja, 2020).The characteristics of activated fluxes are to break into their constituents and vaporize during fusion welding. This flux may be made of oxides or halides. Due to this characteristic, it forms a cover of fumes around the arc. These fluxes create a narrow arc region between the electrode and weld metal by extracting the electron from the superficial region of the arc column. Moreover, these fluxes change the surface tension gradient from negative to positive and therefore the fluids flow in the weld pool in an inward direction. The deviation in the arc construction and geometry of the weld pool enhances the weld penetration in A-TIG welding (Jaypuria, Khandai, Ranjan, & Singh, 2019).

Different researchers have reported the effect of various oxide and halide fluxes for A-TIG welding. Halides have a great electron affinity so it influences the arc constriction only (Leconte, Paillard, Chapelle, Henrion, & Saindrenan, 2007) whereas oxides control the Marangoni convection and arc constriction thus reporting maximum penetration. Kumar and Singh (2017) investigated the effect of oxide flux such as Cr_2O_3, SiO_2, Fe_2O_3, MoO_3, FeO and Al_2O_3on SS 304. Except Al_2O_3, all other flux oxides exhibit a good penetration. Many researchers have reported that the highest D/W ratio was achieved with SiO_2 flux in different grades of steel (Tseng & Hsu, 2011; Shyu, Huang, Tseng, & Chou, 2008). Muthukumaran et al. (2012) patented the activated flux formulation for A-TIG welding of SS 304 LN and 316 LN. The work was tested with 30–50% TiO_2, 25–40% SiO_2, 10–20% Cr_2O_3, 5–15% CuO and 5–15% NiO. Sodium silicate was used as a binder and acetone as a solvent. In the A-TIG welding ratio, the mixture of two or more different powders of

activating flux is important to achieve good penetration depth (Huang H. Y., Shyu, Tseng, & Chou, 2005). The effect of the grain size of SiO_2 on penetration depth in SS 304 was studied by Lu et al. (2003). Small grains of SiO_2 between 0.8 microns and 4 microns have been investigated and it showed a positive effect on the penetration. On the other hand, large grain sizes (25 microns) had no effect on penetration. It has been observed that the smaller flux particles had a larger specific surface area than big particles.

Tanaka et al. (2000) had applied TiO_2 flux on SS 304 plate and it was analyzed that the penetration depth increases sharply with the coating density of TiO_2 flux up to 1 mg/cm^2 and after that it remains constant by increasing coating density. Tseng and Hsu (2011) also studied the effect of the coating density of flux in SS 316 L. It was reported that penetration gets reduced at high coating density due to the high energy requirement to dissolve the high coated flux layer. Ahmadi and Ebrahimi (2015) studied the effect of coating density on D/W ratio on the same material (316 L) with different fluxes. The maximum weld penetration was achieved when the coating densities were 2.1, 2.4 and 3.6 mg/cm^2 with Cr_2O_3, SiO_2, TiO_2 fluxes, respectively. In the case of CaO flux, when the flux density increases, the weld penetration also increases steadily as shown in Figure 2.11.

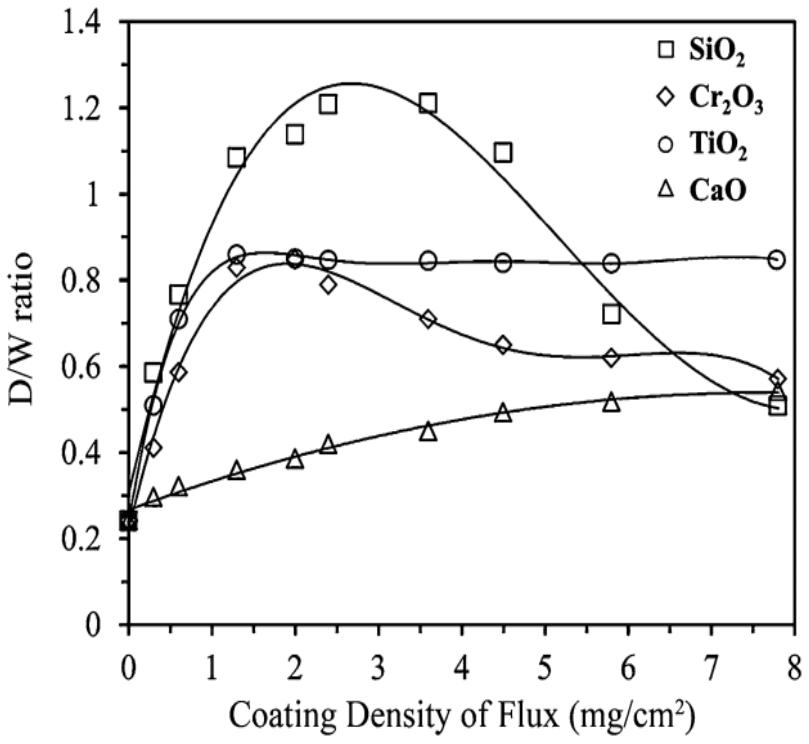

Figure 2.11 Effect of coating density on penetration D/W ratio with different flux (Ahmadi & Ebrahimi, 2015)

Rodrigues and Loureiro (2005) reported the degradation in weld D/W ratio with increase in the thickness of the flux coating since it is difficult to vaporize all the flux during the welding. Thus, all fluxes act distinctly to the arc constriction and the surface tension.

As aforementioned this can be correlated up to some extend with melting and boiling temperatures, grain size, density, composition, thermal stability and electro negativity of fluxes. However, the appropriate correlation between these properties and weld bead geometry is not well identified (Vidyarthy & Dwivedi, 2016). Table 1 has summarized details of the range of various parameters used in the A-TIG welding process.

Table 1 Summarized details of the range of various parameters used in the A-TIG welding process

Material, dimension in mm	Fluxes	Welding current (A)	Arc length (mm)	Torch speed mm/min	Shielding gas and flow rate L/min	Electrode diameter (mm) and angle	Ref.
Gr70 carbon steel and SS 304	TiO_2, ZnO and MnO_2	200	2	55	Argon 12	3.0 60°	(Badheka V. J., 2016)
SS 316L 150 ×150 × 9mm	SiO_2, TiO_2, Cr_2O_3, and CaO	150	3	150	Argon 12	3.2 60°	(Ahmadi & Ebrahimi, 2015)
SS 304L 150 × 150 × 6mm	$TiO_2$and SiO_2	180	3	150	Argon 13	3.2 75°	(Ahmadi, Ebrahimi, & Khosroshahi, 2013)
SS 904L 170 ×55 ×5 mm	SiO_2	140-200	-	140	Argon 18	-	(Ramkumar, Varma, Chaitanya, & S., 2017)
SS 316L 100 ×100 ×6mm	SiO_2, TiO_2, Cr_2O_3, MoO_3, NiF_2, and MoS_2	125-225	3	175	Argon 12	3.2 45°	(Tseng K. , 2013)
SS 304 100× 50× 10 mm	Cu_2O, NiO, SiO_2, CaO, and Al_2O_3	160	3	120	Argon 10	1.6 60°	(Lu, Fujii, Sugiyama, & Nogi, 2003)
SS 304 L 450× 55× 8 mm	TricomponentTiO_2 SiO_2 Cr2O_3	160	3	80	Argon 15	4	(Venkatesan, Muthupandi, & Justine, 2017)
Ferritic/martensitic steel 300 ×150 × 6 mm.	TiO_2	200	2-3	100	Argon, 10-12	2.9 18–20◦	(Vora & Badheka, 2017)
DMR-249A steel 300 × 120 × 10 mm	SiO_2, TiO_2 and other oxide fluxes	120-300	1-4	60-120	Argon, 10	3.2 60^O	(Pamnani, Vasudevan, Jayakumar, & Vasantharaja, 2017)
BS700MC super steel scaled 300 × 150 × 5 mm	CeO_2, B_2O_3,Cr_2O_3, O_4SiTi, NaF	180	3	180	Argon 15	4 60^O	(Cai, Luo, Huang, & Zeng, 2016)
SS 316LN 300 × 234 × 10 mm	oxide flux developed at IGCAR	300	-	60	-	-	(Ganesh, Balasubramanian, Vasudevan, & Vasantharaja, 2016)
Inconel X750	50% SiO_2-50%MoO_3	190	-	75	Argon 15	60°	(Ramkumar, Ramanand, Ameer, Simon, & Arivazhagan, 2016)
SS 304 200 × 100 × 10 mm	-	180	3	120	11-20	2.4 60°	(Morisada, Fujii, & Xukun, 2014)
SS 304 5 mm thickness	Cr_2O_3, Al_2O_3, $KClO_4$	200	3	200	Argon, 10	3.2 60°	(Modenesi, Colen Neto, Roberto Apolinário, & Batista Dias, 2015)
Ferritic SS 409 450x 55x 8mm	TiO_2 ,SiO_2 ,Cr_2O_3	160	-	80	Argon, 15	4mm	(Venkatesan, George, Sowmyasri, & Muthupandi, 2014)

Material, dimension in mm	Fluxes	Welding current (A)	Arc length (mm)	Torch speed mm/min	Shielding gas and flow rate L/min	Electrode diameter (mm) and angle	Ref.
SS 316L 120 × 120× 6 mm.	TiO_2 and SiO_2	175	3	150	Argon 12	3.2 45°	(Tseng & Chen, 2012)
SUS 316L) and hot-roll mild steel (JIS G3131 100 × 50 × 6mm	CaO, Fe_2O_3, Cr_2O_3, and SiO_2	200	3	150	Argon 12	3.2 45°	(Kuo, Tseng, & Chou, 2011)
SS 2205 150 × 130 × 6mm	TiO_2, MnO_2, SiO_2, MoO_3, and $Cr2O_3$	200	2	150	Argon 12	3.2 45°	(Chern, Tseng, & Tsai, 2011)
SS 304 150 × 150 × 5 mm	SiO_2, TiO_2, MoO_3	125	3	75	Argon–Hydrogen mixtures	3.2 60°	(Huang H. , 2010)
SS 304 125× 50 5 to 8 mm	AlF_3, Al_2O_3 Cr_3O_3, CaF_2 Fe_2O_3, NaF Na_2WO_4 ,SiO_2 ,TiO_2	200-300	1-3	200	Argon 10	3.2 60°	(Modenesi, Apolinário, & Pereira, 2000)
P91 steel 100× 25× 6 mm	CaO Fe_2O_3 TiO_2ZnO MnO_2 CrO_3	200	2-3	100	Argon 10-12	2.9 18–20◦	(Dhandha & Badheka, 2015)
SS 309L 100×40×12 mm	ZrO_2 ,CaF_2	110	4	180	Argon 14	-	(Wu, Wang, Zhao, & Peng, 2018)
SS 304LN and 316LN 10and 12mm thickness	Multicomponent	80-280	0.75 and 1.5	60,80, 100,120, 160,200	Argon 10	3 45°	(Vasudevan, Bhaduri, Raj, & Rao, 2007)
SS 316 200×200 mm, 6 mm and 8 mm thickness.	TiO_2	100-350	3	240	100% argon, 95% argon +5% hydrogen, and 50% argon+50 % helium, 8	3.2 60°	(Rodrigues & Loureiro, 2005)

2.5 Optimization of stainless steel A-TIG weld process parameters

To reduce the manufacturing cost without affecting the quality of the products, machine tools need optimized process parameters (Tseng & Hsu, 2011). Also, the relationship and modeling between the process parameters are important not only for the quality of welding but also to understand the intricate relationship between the output and input variables. In the sub- sequent section, several non-traditional optimization methods have been discussed.

A-TIG welding of SS 304 L parameters such as welding current, torch speed and arc gap effect on weld penetration was optimized by Response Surface Methodology (RSM). The generated regression equation was helpful for the prediction of penetration for any random values of selected parameters (Bodkhe & Dolas, 2018). A-TIG of SS 304 LN and 316 LN and alloy steel weld process parameters were optimized by combining the approach of Artificial Neural Network (ANN) and Genetic Algorithm (GA). Two different neural network models were developed to predict penetration and bead width as a function of process parameters for SS 304 LN and 316 LN. To train the back propagation neural network Lavenberg- Marquardt algorithm was used. Optimized neural network architecture comprised four inputs (current, voltage, torch speed and arc gap) and four hidden nodes with one output node (penetration/bead width). The output predicted by the developed ANN model was quite accurate. This developed ANN model was used to form a GA code to obtain target weld bead geometry. The developed GA model optimized the aforementioned weld parameters were validated by performing the experiments and results proved a close agreement between the targeted and the achieved weld bead geometry for both grades of stainless steels (Vasudevan, Arunkumar, Chandrasekhar, & Maduraimuthu, 2010; Chandrasekhar & Vasudevan, 2010). For the same stainless steel grade of alloy, Vasudevan et al. (2007) developed the computational model based on the GA algorithm to optimize the process variables to achieve the desired weld bead geometry after A-TIG welding. A-TIG welded ferritic/martensitic stainless steel's variables such as welding current, torch speed, arc gap and tip angle were optimized using response surface methodology (RSM). A numerical and graphical optimized parameter enhances the penetration of ferritic/martensitic A-TIG welded stainless steel (Vasantharaja &

Vasudevan, 2018). The same multi-objective optimization approach was applied by Korra and Vasudevan (2015) on duplex SS 2205, Korra et al. (2015) on super duplex SS 2507 and Vidyarthy et al. (2018) ferritic stainless steel to achieve the desired weld bead geometry of A-TIG weld. RSM and GA-based model also found accurate to optimize A-TIG welding process parameters. Further, Magudeeswaran et al. (2014) optimized the variables using Taguchi (signal-to-noise analysis) approach to avoid the solidification cracking behavior of A-TIG welded duplex SS 2205. The Taguchi approach was also applied in A-TIG welding of SS 316 L SS parameter optimization to achieve the maximum D/W ratio. Results illustrated that the welding current was the predominant parameter to affect the penetration (Moghaddam & Kolahan, 2019). Ghanty et al. (2008) compared the performance of a fuzzy and neural network- based system for both Multi-Layer Perception (MLP) and Radial Basis Function (RBF) on weld bead features. Dataset was generated with three input parameter welding current, voltage and torch speed on A-TIG welded SS 304 LN and 316 LN. For all sets of data, the fuzzy rule base model depicted the lesser error in prediction of bead width and penetration compared to neural network-based MLP and RBF system. TIG welding of SS 316 L process variables optimized by an integrated approach of RSM and Teaching learning-based optimization (TLBO). In this study, RSM was used to develop the mathematical model and based on this model TLBO approach applied to optimize the tensile strength of TIG welded 316 L (Moi, Rudrapati, Bandyopadhyay, & Pal, 2019). The same way integrated approach of RSM with Jaya and TLBO optimization algorithms were applied to A-TIG welded carbon steel. Both integrated approaches found fairly similar result; however, RSM with Jaya algorithm was found much efficient and simpler due to single phase (Vora, Abhishek, & Srinivasan, 2019).

RSM is found to be the most general and accurate technique to optimize A-TIG welding process parameters of stainless steel alloys. TLBO and Jaya algorithms also have the potential to carry out single and multi-objective optimization, for the A-TIG welding process. However, limited study has been reported in A-TIG welded stainless steel grades of alloys.

2.6 Consequence of process parameters on microstructure and mechanical properties of TIG and A-TIG stainless steel weld

During the welding, increasing the heat input alters the microstructure and thereby mechanical properties of weld metal (Pramanik, Littlefair, & Basak, 2015).The strength of the weld depends on the heat affected zone (HAZ) of weld metal (Vasantharaja, Vasudevan, & Parameswaran, 2019). In A-TIG welding, the amount of liquid molten metal at any point of time is quite low which leads to faster cooling of the weld pool and reduces the size of the weld zone. Moreover, in A-TIG welding fluid motion increases in the molten zone and thereby reduces grain size in weld pool (Berthier, Paillard, & Christien, 2009). Also, the activated flux alters the arc voltage at constant arc current; consequently, a change in heat input influences the microstructure of A-TIG weld joint thereby altering the mechanical properties in A-TIG weld than TIG weld (Vidyarthy & Dwivedi, 2018). The subsequent subsections discuss the microstructure of weld metal which is further followed by mechanical properties of various grades of stainless steel.

2.6.1 Austenitic stainless steel weld

Ahmadi et al. (2013) examined the effect of SiO_2 and TiO_2 flux on microstructures of SS 304 L. It was observed that when the activated flux is applied at a constant weld current, the arc voltage increases thus increasing heat input resulting in the formation of more delta-ferrite in A-TIG weldments than TIG weldments. The presence of delta-ferrite in weld metal reduces the micro crack, refines the particle size, improves the ductility, and also prevents the hot cracking susceptibility of weld (Saluja & Moeed, 2012; Chandrasekar, Kailasanathan, Verma, & Nandagopal, 2017). Tseng and Chen (2012) measured the ferrite content of the weld metal with SiO_2 and TiO_2 flux in SS 316 L by using a ferritoscope. The ferrite content in weld metals increased from 0.5 FN to 3.6 FN during the TIG welding as shown in Figure 2.12(a, b). Due to the fast cooling of the weld metal, the transformation of the ferrite phase to austenite did not take place which resulted in a large part of the metastable delta ferrite structure. The ferrite content in the A-TIG weld metals increased from 0.5 FN to 6.3 FN and 7.2 FN with SiO2 and TiO2 flux, respectively, as shown in Figure 2.13 (c, d). This attributes to the high energy density of the heat source at low heat input during A-TIG welding (Kulkarni, Dwivedi, & Vasudevan, 2019).

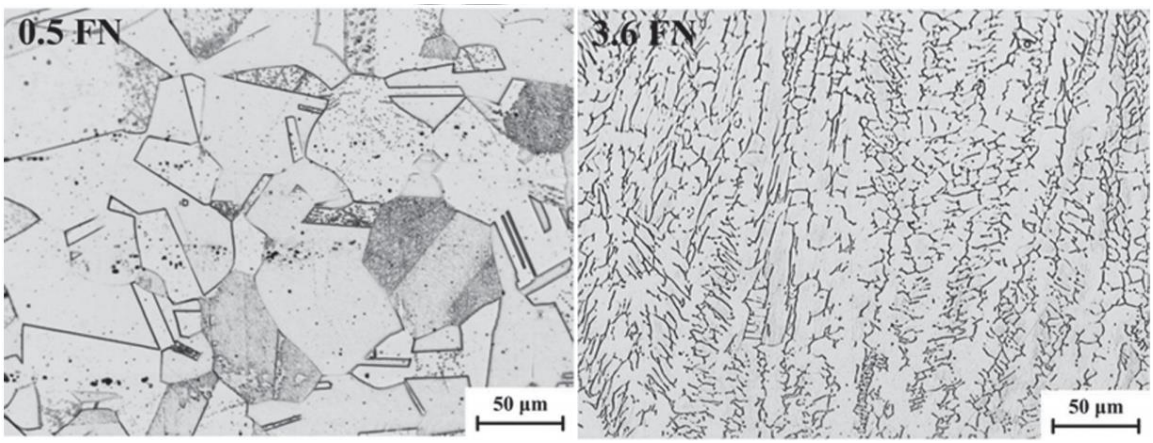

Figure 2.12(a) Base metal 316L SS (b) Weld metal without flux (Tseng & Chen, 2012)

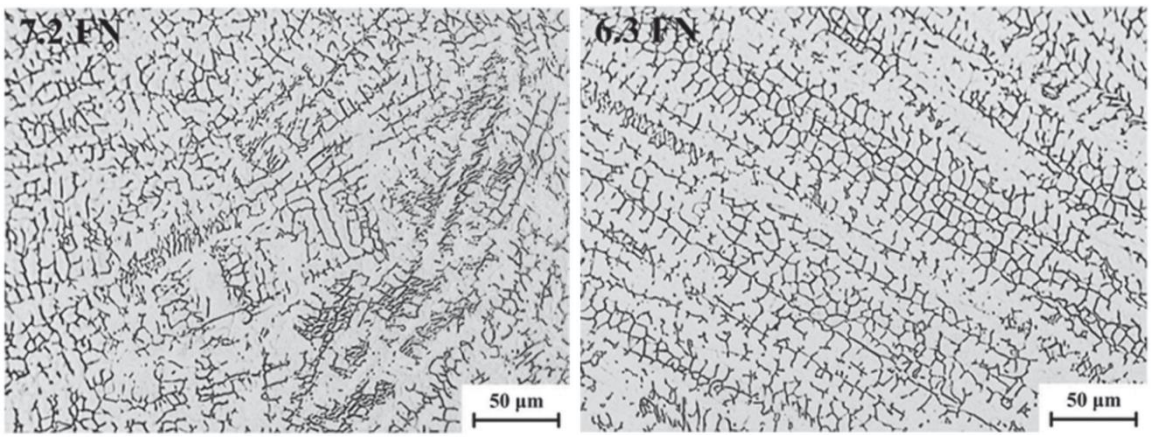

Figure 2.13Weld metal formed with TiO_2 flux (d) Weld metal formed with SiO_2 flux (Tseng & Chen, 2012).

A few researchers also reported higher tensile strength with a slight reduction in elongation owing to higher delta ferrite (BCC structure) in SS 316 L A-TIG weld metal. Also, during A-TIG welding of Carbon steel and SS 304, high tensile strength was reported. This was attributed to the formation of Widmanstatten structure and higher in-grain miss-orientation in weld metal zones (Ahmadi & Ebrahimi, 2015). Tseng et al. (2012) studied the effect of Cr_2O_3 flux on weld geometry of SS 316 L at constant weld parameters. A higher D/W ratio was reported with Cr_2O_3 flux and an improvement in residual stress was reported due to a reduction in heat input per unit length during A-TIG welding. Moreover, hot cracking length measured after TIG welding was 11.8 mm which reduces to 2.3 mm after A-TIG welding as shown in Figure 2.14 (a, b). The susceptibility of hot cracking in weld metal was reduced after A-TIG welding due to the formation of more ferrite content.

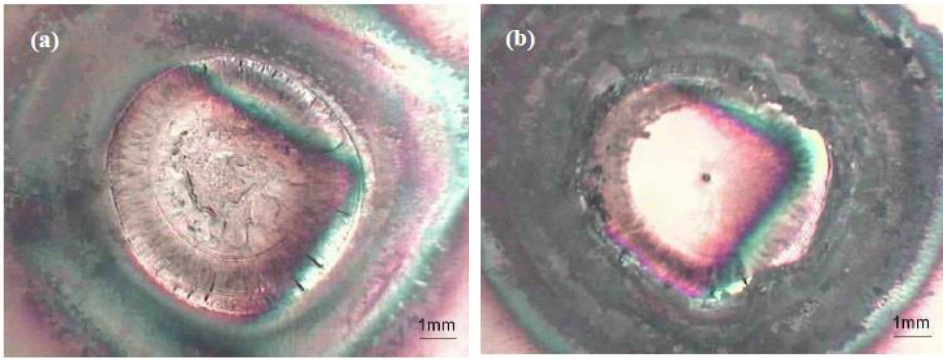

(a) Total crake length 11.8 mm (b) Total crake length 2.3 mm

Figure 2.14 Hot cracking in 316 L (a) with TIG weld (b) with A-TIG weld (Tseng, Chen, & Chen, 2012)

Tseng and Hsu (2011) reported the effect of different fluxes, highest penetration was achieved with SiO2 flux and thus with this flux minimum angular distortion was reported. Also, with an increase in arc voltage, more delta ferrite content was exhibited compared to TIG weld SS 316 L. Vasantharaja et al. (2012) performed TIG welding and A-TIG welding on SS 316 LN plate at preset weld parameters. Lower peak residual stress and distortion was exhibited in A-TIG welding due to intense heat source and absence of filler metal and edge preparation. A similar result was reported in A-TIG welded high tensile strength structural steel (Okano, Tsuji, & Mochizuki, 2017). Shyu et al. (2008) investigated the effect of different fluxes on SS 304 at preset weld parameters. Highest arc voltage was reported with SiO_2 flux thus indicating an improvement in penetration. As a result, effective arc length is increased by 2 to 4 mm and consequently the arc voltage is increased. Moreover, lesser angular distortion with SiO_2 flux was reported due to the high amount of energy concentration during A-TIG welding. Also, higher delta ferrite in A-TIG weld than TIG weld reduces the hot cracking susceptibility. Huang (2010) concluded that the addition of hydrogen in shielding gas reduces the angular distortion in A-TIG and TIG weld metals owing to a higher D/W ratio. Moreover, Huang (2009) added nitrogen in argon base shielding gas, this resulted in strengthening the solid solution and refine the grain of weld metal. This leads to higher tensile strength and hardness in TIG and A-TIG weld in SS 304. However, A-TIG weld exhibit better mechanical properties compared to TIG weld. Also, the hot cracking susceptibility of TIG weld increases with nitrogen addition due to decrease in delta-ferrite content. Kumar et al. (2020) studied the effect of arc length, welding current and speed with multi- component flux on SS 321. Complete penetration was reported with 3 mm arc length, 220A current and 120 mm/min torch speed. Also, higher tensile strength was reported than base metal due to equiaxed dendritic structure with increase in amount of

delta-ferrite after A-TIG welding. However, reduction in toughness was observed than the base metal which was attributed to the oxide flux inclusions and higher delta ferrite content. A similar A-TIG weld study was performed on SS316L at different welding current and torch speed. The maximum penetration was reported with 120A current and 80 mm/min torch speed. Higher tensile strength and micro-hardness were reported than base metal which attributed to higher delta ferrite content and presence of sigma phase in weld zone (Chandrasekar, Kailasanathan, Verma, & Nandagopal, 2017). Vidyarthy et al. (2017) welded dissimilar metal SS 316 L and P91 steel successfully using multi- component flux. Higher corrosion resistance and toughness were reported in 316 LSS due to existence of course grain structure with untampered martensite. However, higher tensile strength and hardness were reported to P91 steel side due to oxide inclusion on 316 L side, and higher dissolution of intermetallic phases in P91side respectively.

2.6.2 Ferritic/martensitic stainless steel weld

Ramkumar et al. (2015) compared the effect of current on SiO_2 and Fe_2O_3 flux and analyzed the microstructure of SS 430 plate. The full penetration was achieved with 160 A current for SiO_2 and with 140A current for Fe_2O_3 flux on 5 mm thick plate. After autogenous TIG welding microstructure analysis exemplified the presence of ferrite, Widmanstatten austenite and martensite clusters as shown in Figure 2.15, where a slight variation in the amount of martensite was reported in A-TIG welding as shown in Figure 2.15(b) this articulated due to difference in cooling rate while using activated flux. The higher hardness and ductility were ascertained with SiO_2 than Fe_2O_3 flux which attributes to the presence of low carbon martensite clusters in the fusion zone.

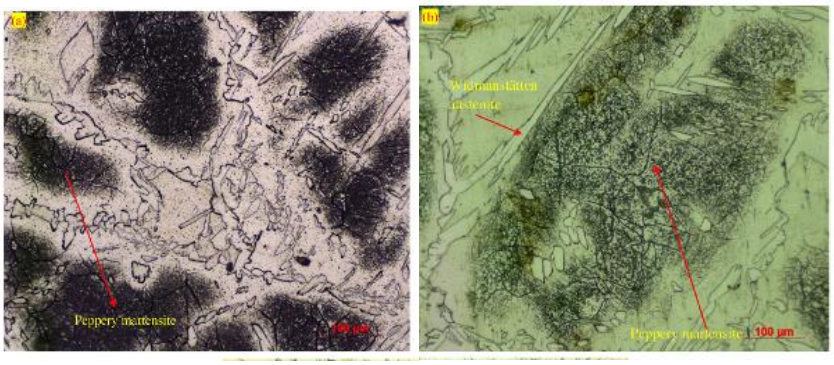

Figure 2.15 AISI 430 Weld metal microstructure after (a) TIG and (b) A-TIG welding (Ramkumar, et al., 2015)

Azevedo et al. (2010) studied the effect of different fluxes on ferritic stainless steel weld. Noteworthy changes were reported in microstructure after A-TIG welding and thereby hardness and impact energy. Vidyarthy et al. (2017) analyzed the effect of SiO_2 flux on A-TIG and Multipass TIG welding of SS 409. Lesser angular distortion was reported with A-TIG than multi pass TIG welding, and this could be attributed to a higher D/W ratio during A-TIG welding. Higher tensile strength was reported with A-TIG and multi pass TIG than base metal but, a significant reduction was recorded in micro hardness with multi pass TIG than A-TIG. This attributes to a change in the microstructure due to several weld thermal cycles. Lower impact energy was observed with A-TIG compared to multi pass TIG due to coarse grain structure, and the presence of oxides and manganese. After A-TIG welding, Post Welded Heat Treatment (PWHT) was performed at 750°C for 2 h followed by air quenching. The impact tested weld metal brittle fracture zone was fully converted into ductile fracture zone after the PWHT as shown in Figure 2.16(a, b). This drastic change was noticed due to the tempering of martensite. Vasantharaja et al. (2019) studied the mechanical properties of TIG and A-TIG welds of ferritic-martensitic (RAFM) steel at a preset weld condition. Higher tensile strength and hardness were reported with A-TIG than TIG welding after the PWHT (760°C) due to a higher amount of dissolved carbon in the martensitic weldment. However, PWHT toughness in A-TIG weld was lesser than TIG owing to higher dissolved carbon in martensite which forms harder martensite. In A-TIG ferritic/ martensitic weld joint the toughness can be increased up to a certain extent by PWHT (2018).

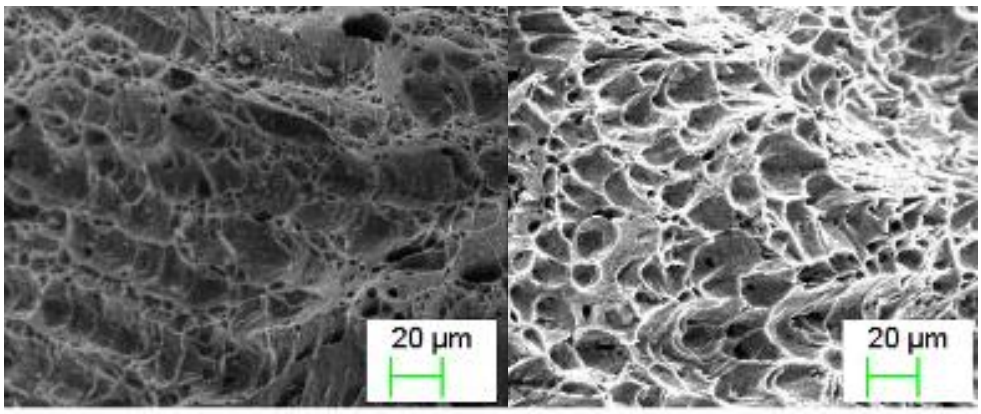

Figure 2.16 Charpy toughness test specimen fracture surface (a)A-TIG (b) A- TIG weld after PWHT (Vidyarthy, Dwivedi, & Vasudevan, 2017)

Vidyarthy and Dwivedi (2017) analyzed effect of welding current, torch speed and coating density on the corrosion behavior of the A-TIG welded SS 409. It was concluded that corrosion

resistance of the fusion zone increases with weld current while it reduces with torch speed and flux coating density. Higher sensitivity to corrosion was measured at the fusion boundary than at the weld centre. The least corrosion rate was recorded with 230A weld current, 120 mm/min weld speed and 1.4 mg/cm coating density. The researchers (Vidyarthy & Dwivedi, 2018; Sakthivel, Panneer Selvi, Parameswaran, & Laha, 2016), also studied the influence of creep behavior at 600°c and 50 N/mm with preset weld parameters on A-TIG and M-TIG welded SS 409. More creep rupture time was depicted with A-TIG weldments than M-TIG weldments. The same result was reported on SS 316 L(N) A-TIG weld (Sakthivel, et al., 2011).

2.6.3 Duplex stainless steel weld

Chern et al. (2011) observed the effect of SiO_2, MoO_3, Cr_2O_3, TiO_2, and MnO_2 flux, on hot rolled 2205 DSS at preset weld parameters. Maximum penetration was observed with MoO_3, Cr_2O_3 and SiO_2 flux and thereby reduces the distortion in the weld metal. Also, an improvement in tensile strength was reported with these fluxes due to reduction in ferrite content after A-TIG welding than TIG welding in 2205 DSS and also in super duplex stainless steel (Saidov, Mourton, Le Gall, & Saindrenan, 2000). In duplex stainless steel, intermetallic phases are reported after the welding, out of which the sigma phase is the most critical one because of its harmful effect on mechanical properties (Paulraj & Garg, 2015). Kumar et al. (2012) reported that depending on the application and weld conditions, metal containing ferrite should be prescribed. The weld joint used in the cryogenic and corrosive environment should have minimum ferrite level (Baelack, Duqette, & Savage, 1979). However, to avoid shot cracking during solidification the ferrite level should be FN-3 to FN-20 but, ferrite level above FN-10 tends to reduce the mechanical properties such as toughness and ductility. Also at elevated temperatures, the delta ferrite transforms into the sigma phase (brittle phase), so it is required to control the ferrite content in the weld metal. Berthier et al. (2009) explored the effect of argon and mixture of argon-helium-nitrogen at different heat input on super duplex A-TIG weld stainless steel.

The penetration increases with heat input in all cases. Maximum penetration was reported argon-helium-nitrogen welding with not much variation in TIG and A-TIG. This attributed to nitrogen addition in shielding gas and grain size reduction in the molten zone. Indeed, corrosion in super duplex stainless steel after TIG and A-TIG welding remains unchanged. From the above review, it can be summarized that heat input is a crucial factor that significantly affects the microstructure of weld metal. Due to the fast cooling of the weld during A-TIG welding, a

higher amount of martensitic structure is formed in ferritic stainless steel. Reduction in ferrite content is reported in duplex stainless steel whereas in austenitic stainless steel more delta-ferrite is formed during A-TIG than TIG welding. A-TIG welding exhibits higher peak hardness and tensile strength in a weld fusion zone than TIG and M-TIG welding in different grades of steel (Sharma & Dwivedi, 2019; Shanmugasundar, Karthikeyan, Ponvell, & Vignesh, 2019). However, in TIG welds, due to auto-tempering effects caused by multi- pass deposition, a higher impact in the toughness was observed. The poor toughness in the fusion zone of A-TIG welding was observed even after the PWHT due to the insignificant response of δ-ferrite to PWHT. Also, residual stress causes cracks to components (Nasir, Razab, Mamat, Iqbal, & Ahmad, 2016). Therefore, to improve the negative effect of residual stress, PWHT can be introduced to increase the component life and weld quality.

2.6 Recent developments in the A- TIG welding process

A-TIG welding process successfully increases the penetration capability up to 400%. (Tathgir, Rathod, & Batish, 2019). But after the A-TIG welding process, entrapped flux particles create a poor weld bead surface appearance which affects the fusion zone profile and consequently the weld quality. To defeat these limitations, alternative welding processes have been suggested by different researchers.

This drawback of A-TIG welding is eliminated by novel chronological advance process called Flux Bounded TIG welding (FB-TIG), along with adopting the benefits of A-TIG welding. This process was first proposed by Sire and Marya in (2001). In this process, the flux was spread on the top surface of the plates to be welded, by keeping small clearance at the centre of the weld pieces as shown in Figure 1.2. Hence, the flux uncovered metal part comes directly in contact with the arc during welding. The mechanism was further elaborated by Jayakrishnan et al. where the activating flux acts as an electric insulator. Due to the insulating effect of flux, the current density increases and produces high penetration depth. Rückert et al. (2007) examined the effect of flux coating thickness in SS 304. A higher weld penetration was observed in A-TIG, than FB-TIG. However, at higher coating thickness equivalent penetrations appear in FB-TIG. Rückert et al. (2014) studied the effect of coating thickness and flux gap and reported that the flux gap played a very crucial role in increasing the penetration. Singh et al. (2017) performed FB-TIG welding by applying ceramic flux on P91 plates. The depth of penetration in FB-TIG increased 2–3 times than TIG welding; however, larger grain size was observed in the welded

and heat-affected zone of FB-TIG which leads to lower hardness. Venkatesan et al. (2017) compared the A-TIG weld with FB-TIG weld on SS 304 L. The penetration depth was slightly lower in FB-TIG welding but it overcomes the other shortcomings of the A-TIG welding process. Based on the theory of arc constriction and modifying the flux coating method, Huang et al. (2012) proposed innovative chronological variant known as Flux Zone TIG (FZ-TIG) welding. In FZ-TIG welding activating flux thermophysical properties with a lower melting temperature, boiling temperature and current resistivity is applied to the central region of the weld line. The activating flux with a higher melting point, boiling point, and current resistivity is applied on the side regions of the weld line before welding. During the welding centre region flux only gets melted and evaporates while outer region flux having higher melting and boiling temperature with higher current resistivity acts as an insulator and contract arc root. The gap between the outer coat flux is filled with centre coat flux as shown in Figure 1.3. The activated flux increases the penetration depth through the three different mechanisms such as the constriction of the arc due to negative particle confirmation theory, insulating layer theory, and reversal of Marangoni convections. FZ–TIG-welded weldments of aluminium alloys, depth of penetration was thrice than that achieved with TIG welding along with improvement in surface appearance. Moreover, enhancement in mechanical properties in aluminum alloys was also reported (Huang, Fan, & Shao, 2012). Rana et al. (2021) reported the comparative study of TIG welding and its variants on oxygen-free copper. The highest D/W ratio was reported in FZ-TIG weld due to strong Reversal Marangoni convection and arc constriction. FZ-TIG welding is the most superior technique than A-TIG and FB-TIG welding. However, no study has been reported on stainless steel alloys, which provides an opportunity for further research.

2.7 Summary of Literature Survey

From the existing literature, a systematic investigation has been carried out to understand the mechanisms and capability of A-TIG weld metal. Research studies concluded that the reversed Marangoni effect and arc constriction mechanisms are responsible for enhanced penetration in the A-TIG welding process. Activated flux having more electro negativity constructs a more constricted arc column. The concentration of surfactants plays a vital role in varying the weld-pool surface-tension gradient and thus penetration. Fluxes used during the A-TIG welding are generally oxides and halides. The fluxes with different chemical composition respond differently to weld bead geometry. Small particles of fluxes show a positive effect on penetration

than large particles. The ratio of a mixture of two or more different powders of activating flux and coating density of flux also plays an important role in weld penetration. The right combination of multi- component activated fluxes can be analyzed on various grades of stainless steel to discover the quality of the weld bead.

Proper selection of process parameters and fluxes is important for good weld bead and effective mechanical properties in A-TIG welding. An increase in welding current promotes the weld penetration but an increase in torch speed and arc length results in a reduction of depth, width and D/W ratio for both high and low sulfur steels. The cross-sectional area at weldment and electron temperature reaches to a maximum value at an electron tip angle of 45°. A larger diameter of the electrode is more suitable due to the high electrode consumption rate in A-TIG welding. The addition of H_2, He, O_2, and N_2 in shielding gas up to some extent increases the heat input which improves the penetration depth. However, the integration of shielding gas at high temperature reacts with activated flux, which may increase the penetration or create a defect in the weld metal. To understand this phenomenon, further experiments need to be performed.

A-TIG welding process parameters are optimized by RSM, GA, ANN, Fuzzy, TLBO and Jaya algorithms to understand the complex relationship between the input and output features that governs the great quality of the weld. The integrated approach of RSM with the TLBO and Jaya algorithms has a greater potential to perform single as well as multi-objective optimization. A-TIG welding exhibits higher peak hardness and tensile strength in the weld metal than TIG welding in different grades of stainless steel. Due to auto-tempering effects caused by multi-pass deposition higher impact toughness was observed in TIG welding than A-TIG welding. PWHT is mandatory to achieve good toughness for A-TIG welding and also recovers the negative effect of residual stress.

A-TIG effectively increases the penetration to a great extent but the entrapped oxide flux forms a high amount of slug on the weld surface and thereby degrades the weld appearance. This drawback is eliminated by FB-TIG welding by adopting the advantages of A-TIG welding up to some extent. However, several parameters such as flux gap, coating density and mechanisms require further understanding for different grades of stainless steel. Deeper penetration depth with good surface appearance is depicted in the FZ- TIG welding of aluminum alloy. Investigation of FZ-TIG welding on stainless steel alloys can be used to develop more sustainable welds.